

# MarineFormer: A Transformer-based Navigation Policy Model for Collision Avoidance in Marine Environment

Ehsan Kazemi<sup>1</sup> and Iman Soltani<sup>1</sup>

**Abstract**—In this work, we investigate the problem of Unmanned Surface Vehicle (USV) navigation in a dense marine environment with a high-intensity current flow. The complexities arising from static and dynamic obstacles and the disturbance forces caused by current flow render existing navigation protocols inadequate for ensuring safety and avoiding collisions at sea. To learn a safe and efficient robot policy, we propose a novel methodology that leverages attention mechanisms to capture heterogeneous interactions of the agents with the static and moving obstacles and the flow disturbances from the environment in space and time. In particular, we refine a temporal function with MarineFormer, a Transformer navigation policy for spatially variable Marine environment, trained end-to-end with reinforcement learning (RL). MarineFormer uses foundational spatio-temporal graph attention with transformer architecture to process spatial attention and temporal sequences in an environment that simulates a 2D turbulent marine condition. We propose architectural modifications that improve the stability and learning speed of the recurrent models. The flow velocity estimation, which can be derived from flow simulations or sensors, is incorporated into a model-free RL framework to prevent the robot from entering into high-intensity current flow regions including intense vortices, while potentially leveraging the flow to assist in transportation. The investigated 2D marine environment encompasses flow singularities, including vortices, sinks, and sources, representing fundamental planar flow patterns associated with flood or maritime thunderstorms. Our proposed method is trained with a new reward model to deal with static and dynamic obstacles and disturbances from the current flow. We evaluate the performance of the proposed deep policy versus the state-of-the-art RL methods and the classical planners. Our method outperforms the existing methods, obtaining 20% improvement over the state-of-the-art baseline model for marine navigation. We attribute the superior performance of the proposed method to several factors including the acquisition of critical sensory information from the environment, optimal design of the network architecture, and the reward functions, tailored to the nature of the obstacles and the environmental disturbances. The project website is available at [https://ehsankf.github.io/MarineFormer\\_web/](https://ehsankf.github.io/MarineFormer_web/).

## I. INTRODUCTION

The main goal of the Unmanned Surface Vehicle (USV) studied here is to overcome disturbances from current flow, avoid obstacles, and reach the goal using the shortest path from the departure point to the destination. Collision avoidance when employing USVs in a dense environment, involving several static and dynamic obstacles, is a challenging problem [1]. In strong currents characterized by flood dynamics, moving agents are heavily influenced by current

flows, leading to complex interactions with both dynamic and static objects. Adherence to the existing protocols [2] for collision avoidance may lead to conflicting actions, particularly in dense marine environments with numerous static and dynamic agents. Maneuvers in marine environment may require deviation from established protocols, especially when interactions with nearby vessels are influenced by strong current forces. In addition, a lack of knowledge of the goal and trajectories of dynamic obstacles presents an additional layer of complexity for the navigation of USVs.

The objective of this work is to propose an obstacle avoidance policy for the marine environment as shown in Fig. 2. Compared with the previous works that ignore the presence of either dynamic obstacles [3] or static obstacles [4], our method considers a heterogeneous environment including static obstacles, moving obstacles as well as strong disturbances due to current flow. In a large-scale oceanic environment, variable ocean currents are more prevalent than dense obstacles. In this work, we assume that noisy information about the flow around the agent can be obtained using satellite imagery, sensors mounted on the USVs, or computational fluid dynamic solvers, although the flow field information farther away from the agent might not be available.

Fig. 1 visualizes the modeled marine environment, where the direction and length of the black arrows correspond to the point-wise direction and magnitude of the current flow, respectively. To represent the large-scale ocean chaos, the simulated currents are characterized by spatially varying distributions of eastward flow with random angles of attack and incorporating singularities such as vortices, sinks, and sources. The vortices cause circulation, and sinks and sources cause strong attraction and repulsion, respectively. As shown in Fig. 1, the yellow circle and the star symbol show the start point and the goal destination of the USV, respectively. The static obstacles such as man-made or natural structures are represented as filled black circles, and empty red circles show the dynamic obstacles which represent other vessels.

We employ two types of sensors on the USV to detect obstacles. The static obstacles are detected by 2D proximity sensors like sonars. The field of view (FOV) of this sensor shown by green beams, primarily covers the front side of the ego-vessel. The field of view (FOV) of the second sensor—potentially a radar, LiDAR, or a combination—designed to detect dynamic obstacles on the water surface, is shown in pink. This sensor typically covers a wider angle to help avoid collisions with vessels. However, the FOV of both sensors can be adjusted as needed. Each

<sup>1</sup>Ehsan Kazemi and Iman Soltani are with the Laboratory for AI, Robotics and Automation, MAE Department, University of California, Davis, CA 95616 USA (e-mail: ekazemi@ucdavis.edu; isoltani@ucdavis.edu).

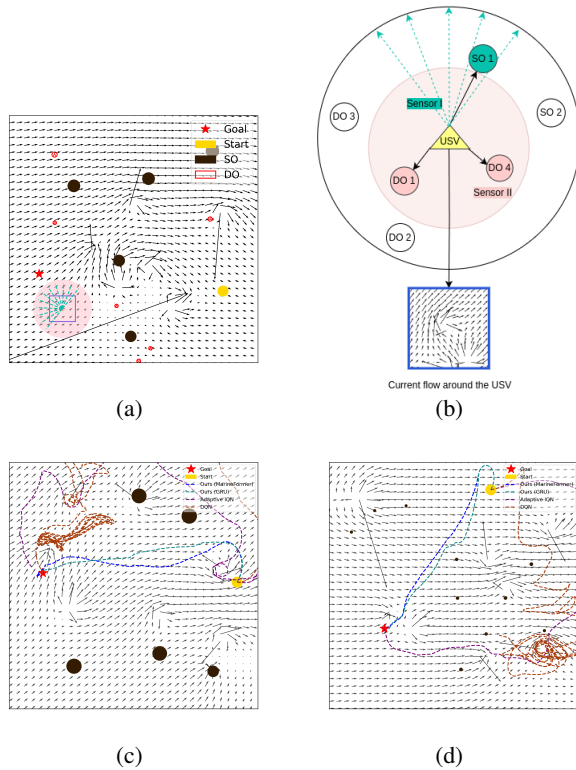


**Fig. 1: The overall overview of the proposed method and comparison of planned trajectories.** Fig. (a) shows the simulated environment. The black arrows show the direction and magnitude of the current flow velocity at each location. (b) The black arrows show the attention of the USV to environmental components. (c, d) Planned trajectories of our proposed path planners and baseline planners.

sensor measures the distance and orientation of obstacles within its respective FOV.

Our method recognizes the heterogeneous nature of underlying dynamical fluid and agent interactions with static and dynamic obstacles. One remarkable characteristic of the marine environment is uncertainty in path planning since the current flow has a significant impact on the navigation trajectory of USVs. Most existing USV navigation approaches overlook the potential benefits of incorporating local current flow observations for trajectory planning, as well as steering and velocity control. Although such measurements are feasible in practice, their exclusion from control and planning reduces flexibility and adaptability, often leading to policy estimation error, unstable trajectories, and an increased risk of collision. In this work, we propose an algorithm that is informed of the local disturbances caused by current flow to enhance the navigation performance of USVs and demonstrate a reduction in the likelihood of collision, travel time, and path length. Our proposed framework integrates the current flow measurements on a grid around the ego-vessel as shown by the blue box in Fig. 1(b). We study how to leverage the information from the local current flow field for the agent to navigate through obstacles while minimally

deviating from the optimal trajectory to the goal.

For autonomous path planning we use Deep Reinforcement Learning (DRL). In recent years, the transformer architecture [5] has significantly impacted the performance of Supervised Learning (SL) over a variety of tasks from computer vision to natural language processing [6], [7], [8], while demonstrating superior performance over traditional architectures such as RNNs and CNNs. The common practice to deal with temporal dependency in DRL with the underlying partial observability problem is to apply recurrent neural networks (RNNs) [9], [10]. Inspired by the recent success in employing transformers in RL and also the deficiencies of RNNs to capture the long-term temporal dependencies, this study focuses on further exploring the benefits of transformers to RL for autonomous navigation tasks in particular for the challenging problem of marine environments involving dynamic and static obstacles and external forces induced by the current flow. Building upon the previous works on crowd navigation [11], [12], we propose a new architecture, MarineFormer, which uses transformers instead of GRUs to capture the temporal correlations.

Our approach uses the ability of attention mechanisms to extract temporal correlation embedded in the current flow measurements, as well as the ego-vessel/obstacles interactions. We use spatio-temporal graphs (sp-graph) for embedding the features of the interaction of robots with environmental disturbances as well as obstacles. In the sp-graph, the link between the agent node and other nodes, i.e., other obstacles is learned using attention models. Our approach seeks to learn an interaction-aware navigation policy that reasons different interactions with the current flow and moving as well as static obstacles as shown in Fig. 1(b). The attention mechanism helps the agent determine the relative importance of each obstacle to the robot while considering the overall flow and avoiding strong disturbances due to singularities in the flow dynamics. This architecture enables the robot to pay more attention to the important interactions for decision-making, especially when dealing with a high number of static and moving obstacles in the presence of nonlinear hydrodynamics leading to overly complex graph dynamics. This approach can better encode the interaction of the agent and the environmental components than directly combining the information of other agents through concatenation or using an LSTM encoder [13], [14].

We use distance measurements of all static obstacle sensors as observations of the deep policy model. The size of the distance measurements is determined by the number of sensor beams and remains consistent regardless of the number of encountered obstacles. In addition, in our setting the number of dynamic obstacles is fixed and a binary mask is used for the obstacles that are not in the FOV of the robot. The robot's belief of the future trajectory of moving obstacles is used to capture the interaction of the robot and the future trajectory of moving obstacles. It was shown previously [15], [16], [11] that incorporating the interactions across moving obstacles can enhance the performance of learning-based methods for obstacle avoidance. By integrating the information from the

subsequently predicted trajectories of moving agents, USV avoids trajectories that might unsafely intersect with those of the dynamic obstacles or can lead to potential collision due to the limited maneuverability of USVs. The partial observation from the local flow is considered as another input feature to the policy model, when transformed into the local coordinate system of the robot. Although DRL has witnessed significant success in recent years, it suffers from the issue of sample efficiency. Using current flow measurement as input can introduce inductive bias which mitigates the sample efficiency problem in DRL. Given the dynamics of the fluid and the presence of moving obstacles, we design a reward function that encourages the robot to balance between avoiding static obstacles and avoiding navigation toward the intended trajectories of dynamic obstacles, while mitigating the risks posed by the attraction forces of sinks. Due to the limited maneuverability of the USV, the reward function proactively discourages the robot from getting too close to obstacles, as avoidance becomes more challenging at short distances.

The main contributions of this paper are as follows. 1) We propose a transformer-based policy network that uses an attention mechanism to effectively capture the spatial and temporal interaction of the robot, obstacles, and an environment with spatially variable hydrodynamics. 2) We propose a method to model the partial information from the flow dynamics surrounding the robot to learn a navigation policy. 3) We propose a new approach to fuse information from sensors that detect dynamic and static obstacles to avoid collisions. 4) A reward function is designed to mitigate the effect of disturbances from the current flow and properly shape the behavior of the ego-agent when coming across other agents or obstacles. 5) We provide a training recipe that enables effective end-to-end policy learning in a highly dynamic marine environment. 6) We compare the proposed policy against state-of-the-art RL-based approaches and conventional reaction-based methods. The results show that by using a reward function that takes into account the local current flow measurements, the future trajectory predictions of dynamic agents, and the likelihood of collision with static obstacles, the navigation safety of USVs in a dense environment is significantly improved. In particular, our proposed approach improves the success rate by 20% compared to the state-of-the-art [17].

## II. RELATED WORKS

Robot navigation in a dynamic environment with external disturbances and obstacles consisting of static and dynamic obstacles has been studied for decades [18], [19], [20], [21]. The path-planning algorithms for USVs can be generally classified into pre-generative, reactive approaches, and learning-based methods. Pre-generative approaches aim to find a safe path avoiding known obstacles and satisfying constraints such as shortest or energy consumption minimization. Previously, researchers have developed diverse geometry-based algorithms such as A\* [22], Dijkstra [23], and FMM [24]; and sampling-based algorithms such as

RRT [25]. Geometry-based methods can generate an optimal path by selecting a suitable heuristic cost function, while computation time grows exponentially with the map resolution. Comparatively, sampling-based methods have a low computational cost, however, they generate nonoptimal and bumpy paths. Conventional reaction-based methods are extensively used for robot navigation and obstacle avoidance. For instance, Artificial Potential Fields (APF) [26] for robot navigation generated repulsive forces to avoid obstacles. Reciprocal Velocity Obstacles (RVO) [27], [28] and Optimal Reciprocal Collision Avoidance (ORCA) [29], [30] improved the performance of velocity collision avoidance approaches [31] in multi-agent navigation problem by applying velocities following reciprocal obstacle avoidance behaviors. OCRA models other agents as velocity obstacles and assumes that agents avoid each other under the reciprocal rules [27], [29]. In addition, both methods are prone to failure if the assumptions such as the reciprocal rule no longer hold [32].

Learning-based methods tackle the issues of reaction-based approaches by learning the interaction in the environment and making decisions. One approach is Deep V-learning methods which uses SL with ORCA as the expert and then uses RL to learn a value function for path planning [4], [13], [14], [33]. However, this approach assumes that state transitions of all agents are known and inherit the same problems as the ORCA expert [12]. To address these problems, decentralized structural-RNN (DS-RNN) uses a partial graph to model the interactions between the robot and obstacles. [12]. Model-free RL is used to train the robot policy without supervised learning or assumptions on state transitions, which achieves better results than ORCA. In [14] a deep policy model based on LSTM architecture is proposed to improve the policy performance when the number of agents is increasing. In [14], [15] higher-order interactions among agents are modeled which consider the interaction of ego-agent and other agents and the indirect effects of interaction among other agents on the ego-agents. Further, in [34] an occupancy grid map is used to encode static obstacle information, improving the obstacle avoidance performance in dense environments. A distributional RL-based method for decentralized multi-agent navigation of USVs is developed in [17]. In their work, it is assumed that the state transitions of all dynamic obstacles are identical, as they follow the same policy. Their studied navigation policy does not take into account the dynamics of environmental disturbances or the future trajectories of dynamic obstacles, resulting in shortsighted behaviors of the robots, as illustrated in Fig. 1. Furthermore, the method relies solely on the current flow velocity measurement at the USV's location as a model-free observation, while the action space is discrete and limited, which restricts the generalization of the approach.

In this work we study transformers as the backbone of the policy architecture. The attention mechanism in transformers does not require a recurrent context input, which makes it ideal for capturing long-term temporal dependencies. RL generally has not advanced beyond shallow GRU models due to challenges by training instability and long training

times because of large number of parameters of large and wide models, such as transformers. Recently, a surge of using transformers has appeared in the RL domain, but it is faced with unique design choices and challenges brought by the nature of RL. In [35], a self-attention framework is leveraged for relational reasoning over state representations. However, in [36], it is shown that vanilla transformers are not suitable for processing temporal sequences and perform worse than a random policy for certain tasks. Gated transformer-XL (GTrXL) [37] proposed to augment causal transformer policies with gating layers with Identity Map Reordering towards stable RL training. Furthermore, [38] suggested a shortcut mechanism with memory vectors for long-term dependency. [39] combined the linear transformer with Fast Weight Programmers for better performance. [36] applied a self-attention mechanism to mimic memory reinstatement for memory-based meta RL. [40] used a transformer with Bellman loss to process observation history as the input of Q-network. Motivated by offline RL, recent efforts have shown that the transformer architecture can directly serve as a model for sequential decisions [41]. Decision transformer [41] learns a policy offline, conditioning on previous states, actions, and future returns, providing a path for using transformers as sequential decision models. There has been a huge effort to improve the scale and training stability of policies. Performer-MPC [42] proposes learnable Model Predictive Control policies with low-rank attention transformers learnable cost functions. In this work, we leverage transformers as temporal encoders. In a similar direction, [43] utilized supervised tasks, while [44], [45] employed pre-trained transformers as temporal encoders. By feeding observations from the current flow, we can mitigate the data efficiency problem often associated with transformers. We demonstrate that transformers outperform GRUs as the memory horizon increases. The problem of poor data efficiency with RL signals can be handled by employing longer episodes, and larger batches in training along with the current flow information.

In large-scale oceanic environments, configurations such as current flows are often more prevalent than dense obstacles. For USV path planning, it is essential to model the effects of uncertainties and external disturbances stemming from environmental factors like ocean currents. In [46], path planning that considers ocean currents is formulated as a multi-objective nonlinear optimization problem with generous constraints. [47] introduced an anisotropic GPMP2 method that employs an energy consumption likelihood function for USV motion planning. [48] utilized motion constraints to reduce the sampling space and superimposed ocean currents on vehicle velocity to update new nodes. [49] derived time-optimal trajectories and strategies by defining and solving the level-set equation for the chasing problem in the presence of dynamic environmental disturbances. In [50] comprehensive ocean information and physical constraints are taken into account to shorten time, improve speed, and save energy. In our work, we use only partial information from the current flow on a grid surrounding the robot.

### III. METHODOLOGY

In this section, we formulate robot navigation as a DRL problem and introduce the reward function. A robot is required to operate in a simulated marine environment and navigate through obstacles and towards the goal upon the availability of sensory information about the obstacles in the FOV of sensors and also given information on the local current flow.

#### A. Approach

Consider a robot navigating in a marine environment with forces from current flow as disturbances and interacting with obstacles including static and dynamic obstacles. We formulate the RL problem as a Markov Decision Process (MDP), defined by the tuple  $\langle \mathcal{S}, \mathcal{A}, \mathcal{P}, \mathcal{R}, \gamma, \mathcal{S}_0 \rangle$ , where  $\mathcal{S}$  and  $\mathcal{A}$  are the sets of states and actions of the agent and  $\mathcal{S}_0$  is the set of initial states of the robot.  $P(s'|s, a)$  is the state transition function that exhibits the dynamics of the environment, which is unknown to the agent due to factors that include the intentions of other agents, noisy sensor measurements, and disturbances from current flow.  $R(s, a)$  is the reward function and  $\gamma \in [0, 1)$  is the discount factor. At each timestep  $t$ , given the observation of current state  $s_t$ , the agent chooses an action  $a_t$ , which leads to the transition  $s_{t+1} \sim P(\cdot | s_t, a_t)$  and the reward  $r_t = R(s_t, a_t)$ . The goal of the agent is to maximize the expected return,  $R_t = \mathbf{E}[\sum_{i=t}^T \gamma^{i-t} r_i]$ , where  $\gamma$  is a discount factor. The value function  $V^\pi(s)$  is defined as the expected return starting from the state  $s$ , and successively following policy  $\pi$ . A common approach to finding the optimal policy  $\pi^*$  in to maximize  $V^\pi(s)$ , and the resulting optimal value function  $V^{\pi^*}(s)$  satisfies the Bellman optimality equation

$$V^{\pi^*}(s) = \mathbf{E}[r_t + \gamma \max_{s_{t+1}} V^{\pi^*}(s_{t+1}) | s_t = s]$$

where  $s_{t+1} \sim P(\cdot | s, a)$  and  $a \sim \pi^*(s)$ .

The robot is considered to reach the predefined goal if its Euclidean distance to the goal is within the threshold  $d_{thres}$  within an episode of length  $T$ . In this work, we assume the dynamic obstacles following the policy of ORCA. The agent assumes constant velocity for dynamic agents to predict their future trajectory. For the marine environment, we consider a planar flow, a uniform velocity featuring a random angle of attack and including singularities such as vortices, sinks, and sources. This simulation setup is more challenging compared to [3], [17] as they only consider flow with vortices. We use the partial information from the current flow, e.g., the velocity of current flow in the near vicinity of the agent, as an observation. The policy model should be able to extract the pattern across spatially variable dynamics of flows that are useful for finding the optimal path to the goal.

At each timestep  $t$ , the policy receives information from the robot's ego-state, including its velocity and location, as well as the goal position, the states of static and dynamic obstacles within the robot's FOV, and the current flow conditions in the vicinity of the vehicle. The observation at timestep  $t$  is expressed as  $\mathbf{S}^t =$

$[\mathbf{S}_{ego}^t, \mathbf{S}_{static}^t, \mathbf{S}_{dynamic}^t, \mathbf{S}_{current}^t]$ .  $\mathbf{S}_{ego}^t$  shows the robot's information given by

$$\mathbf{S}_{ego}^t = [p_x^t, p_y^t, v_x^t, v_y^t, \theta^t]$$

where  $P^t = [p_x^t, p_y^t]$ ,  $V^t = [v_x^t, v_y^t]$  are respectively the position and velocity of the robot at timestep  $t$ .  $\theta^t$  is the heading angle of the robot at timestep  $t$ .  $\mathbf{S}_{static}^t$  contains the information related to reflection from static obstacles in the FOV of the robot,

$$\mathbf{S}_{static}^t = [O_s^{t,1}, \dots, O_s^{t,rb}]$$

where  $rb$  is the number of radial beams emitted from the sensor to detect the static obstacles in the FOV of the sensor and  $O_s^{t,i}$  is the reflection from  $i$ -th beam of the sensor when the robot is in state  $s(t)$ . If no obstacle is detected in the sensor range in the  $i$ -th beam direction, we set  $O_s^{t,i}$  to be twice the sensor range.  $\mathbf{S}_{dynamic}^t$  contains information related to the position and velocity of dynamic agents in the FOV of the agent.

$$\mathbf{S}_{dynamic}^t = [O_d^{t,1}, \dots, O_d^{t,dn}] \quad (1)$$

where  $dn$  is the total number of dynamic obstacles in the environment,  $O_d^{t,i}$  is the concatenation of the current state of the dynamic obstacle  $i$  and the belief of the robot from the future trajectory of agent  $i$ , obtained from the trajectory predictor model. In particular,

$$O_d^{t,i} = [p_{d,x}^{t,i}, p_{d,y}^{t,i}, v_{d,x}^{t,i}, v_{d,y}^{t,i}, \hat{p}_{d,x}^{t+1:t+K,i}, \hat{p}_{d,y}^{t+1:t+K,i}] \quad (2)$$

where  $P_d^{t,i} = [p_{d,x}^{t,i}, p_{d,y}^{t,i}]$ ,  $V_d^{t,i} = [v_{d,x}^{t,i}, v_{d,y}^{t,i}]$  are the position and velocity of the  $i$ -th dynamic obstacle at timestep  $t$ , and  $\hat{P}_d^{t+1:t+K,i} = [\hat{p}_{d,x}^{t+1:t+K,i}, \hat{p}_{d,y}^{t+1:t+K,i}]$  the predicted future trajectory of agent from timestamp  $t+1$  to  $t+K$ . The trajectory prediction can be obtained by simply assuming constant velocity for the dynamic obstacles or using the ground-truth trajectories of agents in distributed centralized multi-agent applications. As we use a fixed-size input for the dynamic obstacles, a binary mask is applied to filter out the dynamic obstacles that are outside the sensor's FOV.

To encourage the agent to account for current flow disturbances and avoid regions with strong currents, we provide the policy model with  $\mathbf{S}_{current}^t$ , representing the current flow velocity on an  $m \times m$  grid in the robot's ego-coordinate system within a rectangular area surrounding the USV.

$$\mathbf{S}_{current}^t = \{(v_{c,x}^{t,i,j}, v_{c,y}^{t,i,j})\}_{i,j=0}^m$$

The outline of the grid is shown in blue in Figure 1. In real applications, noisy measurements of the current flow field can be obtained in various ways including Doppler sensors or even vision cameras [51] or at a larger scale using satellite imagery. Utilizing local observations of the current flow enables the agent to reason about disturbances and avoid high-current regions caused by vortices, or sources, and the risk of being drawn into sinks. These external disturbances can significantly deviate the robot from the optimal trajectory to the target.

## B. Network Architecture

The network architecture for the policy model is shown in Fig. 2. We derive our network architecture from a spatial-temporal graph. Observations of the ego-robot, the seafloor-relative velocity, static obstacles, and dynamic obstacles are transformed into corresponding latent features through attention models. We represent the attention of the robot to dynamic obstacles ( $RD$ ), to sensor reflection ( $RS$ ) and the attention to current flow ( $RC$ ) functions as feedforward networks attention models. We represent the temporal function as a transformer unit  $\text{Tr}$ . In Fig. 2, at each timestep  $t$ , our spatio-temporal graph  $G_t = (V_t, \epsilon_t)$  consists of a set of nodes  $V_t$  and a set of edges  $\epsilon_t$ . The nodes represent the detected static and dynamic obstacles. The edges connect the robot with different detected obstacles and represent the spatial interaction between the robot and the agents at the same timestamp. These interactions are modeled using feedforward attention mechanisms. The obstacles that are not in the FOV of the agent do not integrate into the motion planning.

The attention modules assign weights to each edge that connects to an agent, allowing it to pay more attention to important interactions including obstacles and disturbances from the flow field. The attention is similar to the scaled dot-product attention and is computed using a query  $Q$  and a key  $K$ , and applies the normalized score to a value  $V$ .

$$\text{Attn}(Q, K, V) = \text{softmax} \left( \frac{QK^T}{\sqrt{d}} \right) V \quad (3)$$

where  $d$  is the dimension of the queries and keys. For dynamic obstacles, we use binary masks that indicate the visibility of each obstacle to prevent attention to obstacles that are not in the FOV of the agent. To compute the  $RC^t$  attention at timestep  $t$ , the current flow observation  $\mathbf{S}_{current}^t$  is transformed to the robot coordinate and scaled using  $\tanh$  to the interval  $[-1, 1]$  for stable training. We then apply the convolution layer to obtain the embedding from the flow denoted by  $C^t$ . In  $RC^t$  attention,  $Q_{RC}^t \in \mathbb{R}^{1 \times d_{RC}}$  is the linear embedding of the robot states,  $K_{RC}^t \in \mathbb{R}^{2 \times d_{RC}}$  and  $V_{RC}^t \in \mathbb{R}^{2 \times d_{RC}}$  are linear embedding of the feature  $C^t$ . The attention score is computed from  $Q_{RC}^t$ ,  $K_{RC}^t$  and  $V_{RC}^t$  to obtain the weighted current flow features as in Eq. 3.

Inspired by the Bendy Ruler navigation technique [52] in Fig. 3 we compute the similarity scores across the moving obstacles. The Bendy Ruler technique probes around the robot in multiple directions looking for open spaces and then picks the direction that is sufficiently open while also moving the robot towards the goal. The similarity score is computed as

$$\text{Sim}(V) = \text{softmax}(VDD^TV^T) \quad (4)$$

where  $D$  is a trainable diagonal weight matrix and  $V$  is the linear embedding of the graph related to the dynamic obstacles in the FOV of the robot. This information allows the robot to assign lower navigation priority to areas with dense, cluttered obstacles, where the probability of collision is higher. It is important to note that as the visibility of

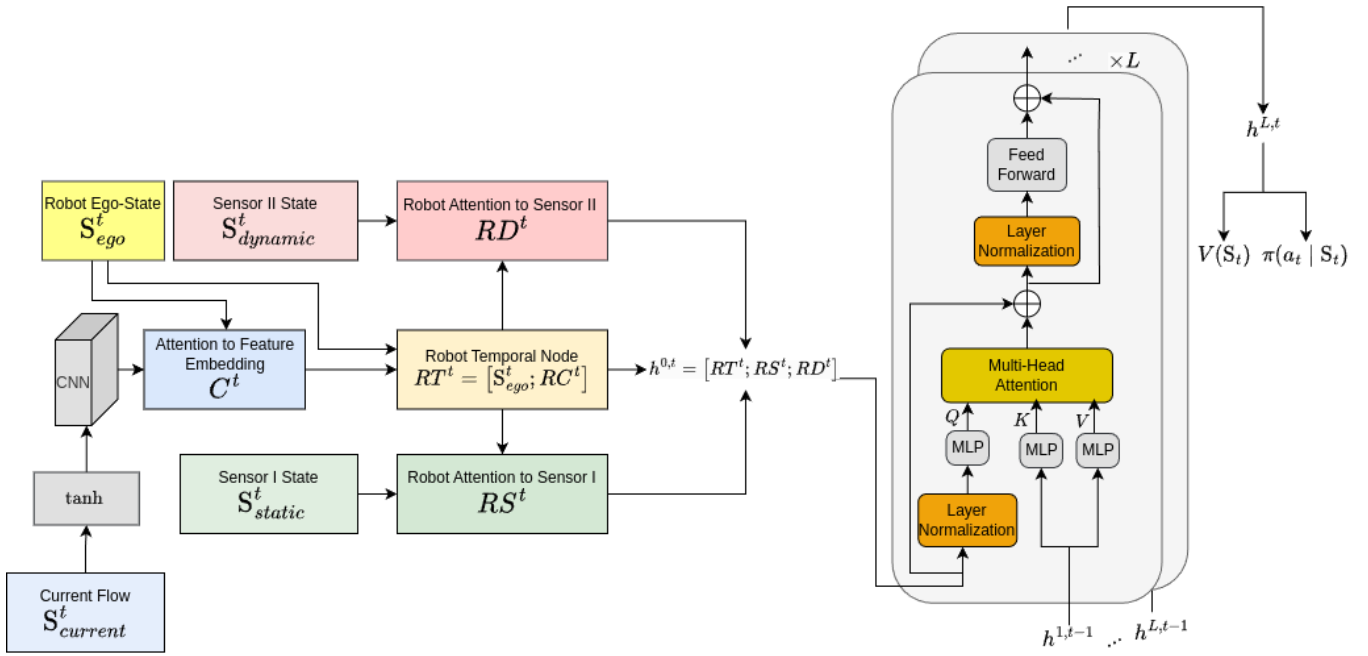


Fig. 2: The overall architecture of our proposed interaction graph and MarineFormer architecture.

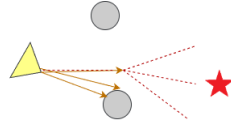


Fig. 3: The schematic of Bendy Ruler algorithm.

obstacles changes due to the movement of agents, and external disturbances fluctuate with the spatially varying current flow, the set of nodes  $V_t$  and edges  $\epsilon_t$  and the parameters of interaction function may change correspondingly. For this purpose, we include the temporal correlation of graph  $G_t$  in different timesteps using another function denoted by the transformer module in Fig. 2. The input to the temporal function of navigation policy is composed of the attention graphs, obtained from computing the robot's interaction with the environment. This embedding, denoted by  $A^t = [RC^t, RS^t, RD^t]$  in the latent space, provides information for long-term decision-making by prioritizing the obstacles and navigation paths. For example, the robot might give a lower priority (lower desirability) to high circulating flow regions of the environment and try to move through the regions that are located near calmer flow conditions. The temporal function links the graphs across consecutive timesteps, overcoming the short-sightedness of reactive methods and enabling the robot to make long-horizon decisions. Our natural goal of using transformers is to use it as a temporal sequence encoder [37], [43]. The latent features from the observations are transformed into corresponding temporal features using this encoder:

$$h^{l,t} = \text{Emb}_{0:t} = \text{Tr}(h^{l,0}, \dots, h^{l,t}),$$

where  $l = 1, \dots, L$  and  $\text{Emb}_{0:t}$  represent the embedding of historical from initial observation to current observation. Finally, the  $h^{L,t}$  is fed to a fully connected layer to obtain the value  $V(s_t)$  and the policy  $\pi(a_t | s_t)$ . Following the stream in Fig. 2, the transformer for the temporal function is composed of a stack of  $L$  identical layers, denoted as  $\text{Tr}^l$  for the  $l$ -th layer. Each layer has two sub-layers. The first is a multi-head cross-attention mechanism between  $h^{l-1,t}$  and the output of  $l$ -th layer from the previous timestep  $h^{l,t-1}$  and the second is a simple, fully connected feed-forward network. We employ a residual connection around each of the two sub-layers, preceded by layer normalization. That is, the output of each sub-layer is  $x + \text{Sublayer}(\text{LayerNorm}(x))$ , where  $\text{Sublayer}(x)$  is the function implemented by the sub-layer itself. All the  $L$  layers produce outputs of the same dimension. Coupled with the residual connections, there is a gradient path that flows from output to input without any transformations. At each timestep, the  $h^{l-1,t-1}$  and  $h^{l,t}$  are passed to the  $l$ -th layer of transformer for  $l = 1, \dots, L$

$$h^{l,t} = \text{Tr}^l(h^{l,t-1}, h^{l-1,t})$$

where  $h^{l,t-1}$  is the hidden state of the  $l$ -th layer of transformer at time  $t-1$  and  $\text{Tr}^l$  is the  $l$ -th layer of  $\text{Tr}$ . For  $t=0$  we assume  $h^{*,t-1}$  is an arbitrarily-obtained input embedding, e.g., the embedding from observation in the RL environment per-timestep. Since  $h^{l,-1}$  is chosen arbitrarily, to ensure it does not introduce a biased gradient to the attention model, we align  $h^{l,-1}$  and  $h^{l-1,0}$  by setting the initial feature values for current flow to zero. This guarantees that the starting point does not contribute misleading information to the model's learning process, thereby maintaining unbiased gradient flow through the network and stabilizing the training. We demonstrate in the experiments that our

architecture has stability and performance that surpasses the baseline models.

### C. Reward Function

The reward function is defined as follows

$$r_t = \mathbf{1}_{collision}(s_t)r_{collision} + \mathbf{1}_{goal}(s_t)r_{goal} + \mathbf{1}_{collision^c \cap goal^c}(s_t)(r_{pot,t} + r_{do,t} + r_{so,t} + r_{cg,t} + r_{ck,t} + r_{cs,t}) \quad (5)$$

$\mathbf{1}$  is the indicator function, and  $r_{collision}$  and  $r_{goal}$  are given when the agent in the state  $s_t$  reaches the goal or has a collision with any obstacles, respectively. The indicator function  $\mathbf{1}_{collision^c \cap goal^c}$  is defined for states  $s_t$  that are in neither the collision state nor the goal state. In addition, we add a potential-based reward  $r_{pot} = f_{step}(dist^{g,t-1} - dist^{g,t})$  to guide the robot to approach the goal, where  $dist^{goal,t}$  is the  $L_2$  distance between the robot position and goal position at time  $t$ . The factor  $f_{step}$  is a hyperparameter that is set during training. Due to the limited maneuverability of USVs with differential drive in marine environments, proximity to obstacles poses a high risk of collision in subsequent steps. To discourage the robot from encroaching the obstacles, we use the rewards  $r_{do,t}$  and  $r_{so,t}$  to penalize such intrusions:

$$r_{do,t} = \min_{i=1,\dots,dn} \min_{k=1,\dots,K_{do}} \left( \frac{\mathbf{1}_i^{t+k} r_{collision}}{2^{k+2}} \right) \quad (6)$$

$$r_{so,t} = \min_{i=1,\dots,rb} \min_{k=1,\dots,K_{so}} \left( \frac{\mathbf{1}_i^{t+k} r_{collision}}{2^{k+2}} \right)$$

$\mathbf{1}_i^{t+k}$  indicates whether the robot collides with  $i$ -th obstacle or in the direction of  $i$ -th radial beam of the sensor at the predicted position at the timestep  $t+k$  and  $r_{collision}$  is the penalty for collision. We assign different weights to the intrusions at different prediction timesteps, allowing the robot to incur a smaller penalty for intruding into the obstacle zones that are farther in the future. The main difference between  $r_{do,t}$  and  $r_{so,t}$  is that for computing  $r_{do,t}$  we take into account the predicted trajectory of dynamic obstacles for potential collision, while for  $r_{so,t}$  we only use the information from the dynamics of the robot to predict a potential intrusion with the zones of static obstacle in the future. In summary, we hypothesize that when faced with complex obstacles that are difficult to avoid given the robot's limited maneuverability, adopting a proactive policy and maintaining distance from those obstacles is the most effective approach. The definition of the rewards  $r_{do,t}$  and  $r_{so,t}$  are inspired by the Bendy Ruler algorithm, illustrated in Fig. 3, which probes the area around the robot in multiple directions to identify open spaces while progressing towards the target. This is also similar to the concept of velocity obstacles [31], which identifies the set of velocities leading to a future collision with static and dynamic obstacles. The attraction force from sinks can lead to a stagnation problem where thrusters may be unable to generate enough force to escape, hence, trapping the agent at the center of the sink. To discourage being trapped in the attraction zones, we design the reward component  $r_s$  to penalize the robot when it fails

to move closer to the target by at least a threshold distance  $\bar{d}$  within two consecutive timesteps:

$$r_{disp,t} = \begin{cases} -0.2 & \text{if } r_{pot,t} < \bar{d}_r, \\ 0 & \text{otherwise.} \end{cases} \quad (7)$$

## IV. EXPERIMENTS

In this section, we conduct various obstacle avoidance experiments. Our 2D simulation environment simulates a robot navigating in a dense obstacle condition in Fig. 1.

### A. Experiment Setting

We consider two training scenarios as shown in Fig. 1; the first scenario (Fig. 1c) consists of 10 dynamic obstacles and 5 static obstacles. The second scenario (Fig. 1d) consists of 25 dynamic obstacles and 10 static obstacles. The range of radius of static obstacles in Scenario I is chosen randomly from the interval  $[1.0, 1.5]m$ , and the range of static obstacles for Scenario II is randomly selected from the interval  $[0.2, 0.3]m$ . In other words, the size of static obstacles for Scenario I is on average 5 times bigger than Scenario II. All dynamic obstacles are controlled by ORCA and react to other dynamic obstacles, not the robot. This prevents the robot from learning a policy that considers dynamic obstacles yielding to it during the navigation. The radius of dynamic agents is set to  $0.3m$  with the preferred velocity of  $2m/s$  and FOV of  $2\pi$  rad. We assume the dynamic obstacles occasionally are changing their goals to other random positions within an episode and current flows do not impact the trajectory of dynamic obstacles. Our environment is denser concerning the number of obstacles compared to previous work [3], [17] as we consider 10 static obstacles and 25 dynamic obstacles in a rectangle of size  $40m \times 40m$  versus 8 static obstacles in an environment of size  $50m \times 50m$  in their experiments. Therefore, our simulated environment sets forth a more challenging collision avoidance problem and upon successful training leads to a more interactive navigation policy.

The simulated current flow is generated from the interaction of uniform flow, vortices, sinks, and sources. The arrows as shown in Fig. 1 denote the velocity vector of current data at the start position of each arrow. We apply the interpolation between two adjacent nodes to compute the current flow at each point. In each episode, the starting and the goal position of the robot, the location of obstacles, the angle of attack for the uniform flow, and the distribution of flow singularities, i.e., vortices, sinks, and sources, are randomly initialized. The uniform flow has a magnitude of  $V_{inf} = 1m/s$  with a random angle of attack chosen from the interval  $[0, \pi/4]$  rad. The velocity of the current flow is simulated using potential flow techniques with vortices [53]. For each environment, we generate 4 vortices 4 sinks, and sources. The intensity of vortices, sinks, and sources are chosen randomly from the interval  $[5\pi, 10\pi]$  rad. The centers of flow singularities are chosen so that the distance of each paired singularity is greater than the sum of the radius corresponding to the velocity threshold of  $1m/s$  at the interaction point. These

randomly generated flow singularities pose extra challenges for learning a policy that can generalize to varying current disturbances.

### B. Kinematic of USV

The kinematic model in [54] is used to model the dynamic of the robot in the existence of current flow as follows

$$\frac{d\mathbf{X}(t)}{dt} = \mathbf{V}_{tot}(t) = \mathbf{V}_{curr}(\mathbf{X}(t)) + \mathbf{V}_S(t) \quad (8)$$

where  $\mathbf{V}_{tot}(t)$  is the total velocity of robot,  $\mathbf{V}_{curr}(\mathbf{X}(t))$  is the current flow velocity at robot position  $X(t)$ , and  $\mathbf{V}_S(t)$  is the steering velocity of robot. I.e., we superimpose the ocean current on the vehicle steering velocity to update the total ground velocity of the vessel. We assume differential drive kinematics for the simulated USV. The robot action at timestep  $t$  is  $\mathbf{a}_t = (\Delta v_t, \Delta \theta_t)$ , where  $\Delta v_t$  is the change in the robot steering speed or equivalently the magnitude of  $\mathbf{V}_S(t)$ , and  $\Delta \theta_t$  is the change in the heading of the robot. The navigation policy is described as  $\pi : \mathbf{S} \rightarrow (\Delta v_t, \Delta \theta_t)$ . The action space is continuous and  $\Delta v_t$  and  $\Delta \theta_t$  are capped based on the specifications of the thrusters of the USV. In the experiment, we choose the control timestep  $\Delta t = 0.25s$  and cap acceleration by clipping the change of velocity at each timestep i.e.,  $\Delta v_t$  to the range  $[-0.1, 0.1]m/s$ . Similarly, rotational acceleration is capped by clipping the change of heading i.e.,  $\Delta \theta_t$  to the range  $[-0.1, 0.1]$  rad. The steering speed is clipped to  $[0, v_{pref} = 2m/s]$  at the inference time. During training we allow the velocity to become negative but we add a penalty for generating a negative velocity. During the inference time, we clip the negative speeds of the robot to zero to rule out the possibility of the robot going backward. The actions are used to update the steering speed of the robot, with the following equations:

$$v_s[t+1] = v_s[t] + \Delta v_a$$

$$\theta_s[t+1] = \theta_s[t] + \Delta \theta_a$$

and therefore the steering velocity  $\mathbf{V}_S(t+1)$  is obtained as follows

$$\mathbf{V}_S(t+1) = [v_s[t+1] \cos(\theta_s[t+1]), v_s[t+1] \sin(\theta_s[t+1])]$$

The action space in our method is continuous while the prediction-based method in [3], [17] is restricted to a small discrete set of predefined linear acceleration and angular velocity. We assume that the sensor for detecting static obstacles has 11 beams, spanning a FOV of  $\pi$  rad with a  $5m$  detection range. FOV of sensor II for detecting moving obstacles is  $2\pi$  rad, again with a sensor range of  $5m$ . These sensors represent a 180-degree sonar and a 360-degree LiDAR, similar to those typically mounted on USVs in real-world applications. We assume constant velocity to predict the trajectory of dynamic obstacles in Eq. 2 along a straight line along the current heading. We feed the information of current flow on a  $8 \times 8$  rectangular grid of size  $5m \times 5m$  surrounding the vessel to the neural model after transforming the velocity measurements to the ego-coordinate of the robot.

### C. Baselines

We compare our approach with two reaction-based methods: We use ORCA as a baseline where the agents avoid each other under the reciprocal rule [27], [29]. Although ORCA accounts for mutual interactions among agents, the hyperparameters are sensitive to crowd behaviors and thus need to be tuned carefully to ensure good performance [55]. We also choose one classical local planning method as a baseline, which is an Artificial Potential Field (APF) method [56]. This approach constructs an attractive potential field  $U_{att}$  and a repulsive potential field  $U_{rep}$  to generate forces that guide the robot toward its goal while repelling it from obstacles. For a given observation, the repulsive force is the sum of contributions from all obstacles. To output an action decision consistent with the robot's differential drive kinematics, we compute the angle difference between the total force  $\mathbf{F}$  and the robot's velocity. This difference is then mapped to the angular velocity that results in the closest angle change in one control step. Additionally, we project  $\mathbf{F}$  in the direction of the robot's velocity, scale it by the reciprocal of mass ( $1/500$ ), and map it to the closest linear acceleration.

We also compare the performance of our model with learning-based approaches for collision avoidance for USVs. We choose the method in [17] as a baseline. Their work is based on implicit quantile networks (IQN) [57], which expresses the return distribution with a quantile function  $Z_\tau := F_Z^{-1}(\tau)$ , where  $\tau \sim U([0, 1])$ , and enables the incorporation of a distortion risk measure  $\beta : [0, 1] \rightarrow [0, 1]$  to compute a risk distorted expectation  $Q_\beta(s, a)$  as well as a risk-sensitive policy  $\pi_\beta$ . In Distributional RL [58], the return distribution  $Z^\pi(s, a)$  is learned, where  $Q^\pi(s, a) = \mathbf{E}[Z^\pi(s, a)]$ , and the Bellman equation for distribution of return turns to

$$Z^\pi(s, a) = R(s, a) + \gamma Z^\pi(s', a').$$

The RL model is trained using IQN loss which is constructed from quantile Huber loss. The control timestep in this baseline is  $\Delta t = 0.05$ , and the linear acceleration  $a$  and angular velocity  $\omega$  are selected from the intervals  $a \in \{-0.4, 0.0, 0.4\}m/s^2$ , and  $\omega \in \{-0.52, 0.0, 0.52\}rad/s$ . As the control timestep for the baseline approach is 5 times smaller than ours, we selected comparable bounds for  $\Delta v_a$  and  $\Delta \theta_a$  in our approach to ensure a fair comparison. We choose DQN [59] as the traditional DRL baseline, and use the implementation from [59]. DQN represents the action-value function as a neural network model  $Q(s, a; \theta)$ , and learns the network parameters  $\theta$  by optimizing the loss  $\mathcal{L}_{DQN}$  computed with samples in the format of  $(s, a, r, s')$  from experiences as follows

$$\mathcal{L}_{DQN} = \mathbf{E}[(r + \gamma \max_{a'} Q(s', a'; \theta^-) - Q(s, a; \theta))^2]$$

We also use GRU in place of the transformer for the temporal function to demonstrate the benefits of using the transformer as a temporal encoder in MarineFormer.

#### D. Training Configuration

The number of attention heads for  $RC$ ,  $RD$ , and  $RS$  is set to 1, and the number of layers  $L$  in Tr in MarineFormer is 1. For the reward function (5), we set  $r_c = -20$  as the penalty of collision and  $r_g = 10$  as the reward for reaching goals.  $K_{do}$  and  $K_{so}$  in (6) are set to 5 and 3 respectively. We set  $\bar{d}_r$  in Eq. (7) to 0.2. In each step, the experience tuple  $(s, a, r, s')$  of the robot is inserted into the replay buffer  $\mathcal{M}$ . We use PPO, a model-free policy gradient algorithm for policy and value function learning [60]. In the PPO we set the coefficient of value loss to 0.5. We perform training in 32 processors (environments). At the beginning of every training episode, a new training environment is generated. The goal point, the location of static obstacles, and the initial position of dynamic agents are randomly generated. We assume at least  $12m$  distance between the start point and the goal location and the obstacles are separated by  $5m$ . The number of updates for each environment is 125000 with 45 steps for each environment to fill the replay buffer. Data are sampled without replacement from the replay buffer to complete one full epoch to avoid overfitting. The episode ends if the robot reaches the goal, collides with an obstacle or the episode takes longer than the pre-set time limit. The time limit of each episode is set to  $110s$  which is equivalent to 440 steps. We set the length of PPO epochs to 5 and the number of mini-batches is 2. Therefore, the batchsize is obtained as  $(32 \times 45)/2$ . To train all versions of RL policy, we use Adam with learning rate  $4e - 5$ ,  $\beta_1 = 0.9$ ,  $\beta_2 = 0.999$ , and  $\epsilon = 1e - 5$  without weight decay, and we clip the global norm of the gradient at 0.5. The entropy coefficient after 15000 updates increases linearly to encourage the agent for sufficient state-space exploration and enhance the error recovery.

#### E. Evaluation

In this section we conduct the experiments on the simulation scenarios described earlier to show the benefits of our proposed approach in incorporating local observations of current flow in decision-making, employing Tr architecture for temporal function, applying the similarity scores across dynamic obstacles, and the effectiveness of trajectory prediction for better maneuverability of USV in avoiding obstacles. We evaluate our proposed model and the baseline approaches in two scenarios, shown in Figs. 1c and 1d. Both scenarios contain dynamic and static obstacles. We test all methods with 500 random unseen test cases. The navigation metrics measure the quality of the navigation and include the percentage success rate (SR), and path length (PL) in meters for all the episodes including failed episodes. The success rate is defined as the percentage of successful test episodes. If the robot cannot reach the goal within the episode time limit or it collides with an obstacle, the test episode is considered failed. The path length is defined as the length of the trajectory traversed by the agent to reach the goal.

In Tab. I we compare the baseline methods and our proposed method. For the method indicated by the star symbol, we add zero mean Gaussian noise with a standard deviation

Method	Scenario I		Scenario II	
	SR	PL	SR	PL
APF	62%	201.84	60%	195.23
ORCA	7%	112.46	5%	105.57
DQN	68%	106.98	69%	83.77
Adaptive IQN	70%	60.73	70%	94.28
Ours (GRU)	86%	61.90	85%	63.86
Ours (GRU)*	84%	63.02	79%	66.19
Ours (MarineFormer)	90%	61.94	<b>86%</b>	<b>61.81</b>
Ours (MarineFormer)*	<b>91%</b>	<b>60.71</b>	81%	64.40

TABLE I: **Overall trajectory prediction accuracy.** The best result is shown in bold font.

of 0.1 to the velocity field of current flow observations during training to examine the robustness of our RL policy to the noisy measurements of the current flow. Tab. I shows that our method achieves the highest success rates across different levels of environment complexity. The results show that the Adaptive IQN is plateauing at the success rate of 70% and MarineFormer increases SR of Adaptive IQN by around 20% and 16% for scenarios I and II, respectively. The results from Adaptive IQN are comparable with DQN and they marginally improve the reaction-based model APF. The results from ORCA show the lowest success rate as it does not account for the environmental disturbances from the current flow. Almost all the methods in Tab. I show lower SR for Scenario II compared to Scenario I. The reason is that the environment in Scenario II is more densely populated with obstacles, making navigation significantly more challenging. The MarineFormer significantly improves the PL across all methods for Scenario II. The results also show that using Tr as a temporal function leads to better policy compared to using GRU in both scenarios. In addition, as the noise in current flow measurement increases, Ours (MarineFormer)\* shows better robustness compared to Ours (GRU)\*. This indicates that applying a more expressive method for the temporal encoder leads to higher SR for path planners.

The navigation trajectories of 8 sample cases for learning-based methods are compared in Fig. 4. In Fig. 4a, the trajectory of our proposed method is less affected by current flow disturbances at the start point, whereas using Adaptive IQN and DQN, the USV is disturbed by the external current forces. As the navigation progresses, MarineFormer successfully maneuvers between two static obstacles, while the trajectory of the GRU-based method is disrupted by the upstream source, ultimately leading to a collision. In Fig. 4b, MarineFormer demonstrates more controlled steering around obstacles compared to other methods. The steering angle for obstacle avoidance in Adaptive IQN is excessively large, increasing the path length and ultimately leading to a collision with a dynamic obstacle before reaching the goal. In Figs. 4c and 4d the trajectories of Adaptive IQN and DQN agents are highly affected by flow disturbances exerted by vortices, ultimately trapping them in the vortex with no ability to escape. Fig. 4d indicates that, unlike the greedy behavior of baseline methods, our method can effectively find

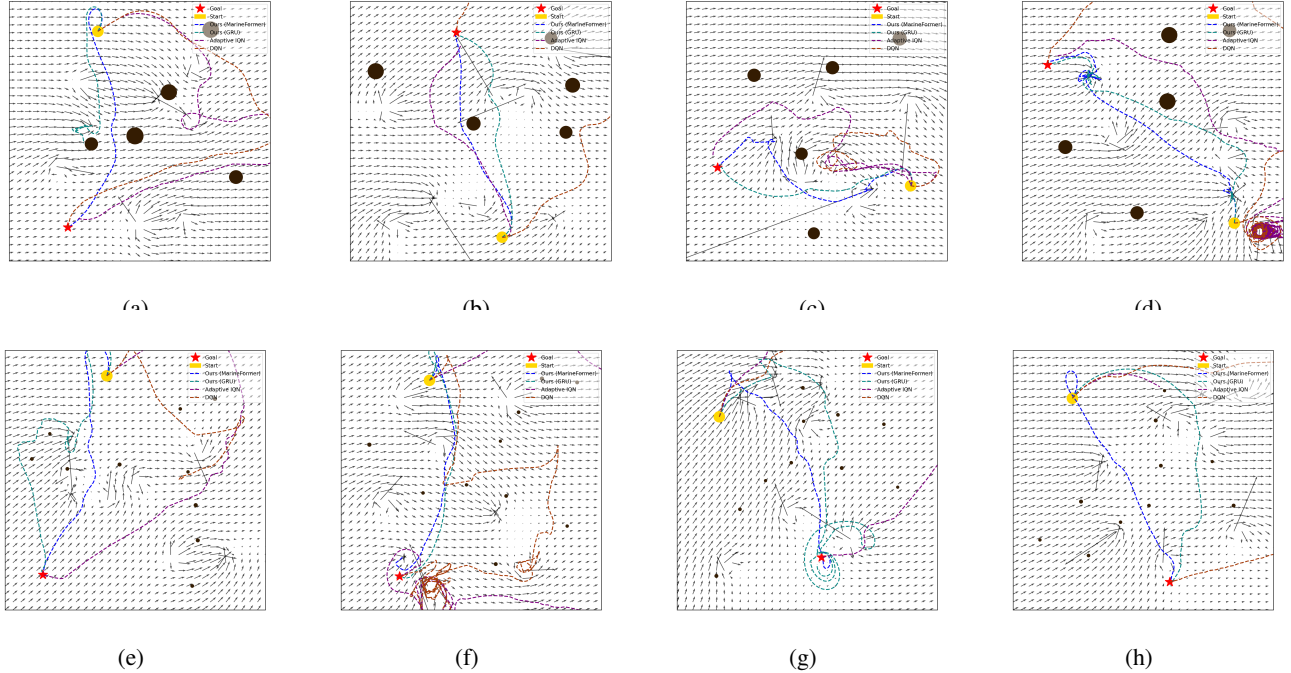


Fig. 4: **Planned trajectories.** Trajectories of Ours (MarineFormer), Ours (GRU), Adaptive IQN, and DQN for different representative environmental settings. The top row shows the results related to Scenario I and the bottom row shows the results related to Scenario II.

a balance between avoiding collisions and not being trapped in circulations caused by vortices. In Fig. 4d, the agents, utilizing our proposed policy, are temporarily trapped by the pull force of a sink but ultimately manage to escape and proceed toward the goal. Fig. 4e shows that almost all the agents successfully reach the target, however, the trajectory of MarineFormer is the least affected by the disturbances from current flow. Fig. 4f exhibits several vortices along the path from the start point to the goal. The result shows that the vortices do not impact the trajectory of our proposed method while significantly influencing the trajectories of baseline agents. Fig. 4g displays an environment with complex hydrodynamics, featuring a sink near the start point and a source close to the goal, along with several singularities along the path. The results demonstrate that the high-intensity flow at the start point significantly deviates from the baseline agents. At the target point, the behavior of the GRU method is heavily influenced by the source. Fig. 4h shows a vortex close to the goal which shows no effect on the navigation path of our agents. The results conclude that the policy learned by our methods and in particular, MarineFormer enables proactive and long-sighted robot decision making especially in challenging navigation tasks in marine environments in the existence of current flow disturbances.

#### F. Ablation Study

In this section, we conduct an ablation study on the impact of the different components of our proposed method. Tab. II shows that how systematically removing specific elements

$r_{do,t}$	$r_{so,t}$	$r_{disp,t}$	similarity score	current flow observation	SR	PL
✓	✓	✓	✓	✓	90%	63.94
✗	✓	✓	✓	✓	71%	65.33
✓	✗	✓	✓	✓	77%	63.95
✓	✓	✗	✓	✓	65%	67.50
✓	✓	✓	✗	✓	83%	62.82
✓	✓	✓	✓	✗	71%	70.40

TABLE II: **Ablation study.** Ablation study on the components of the proposed method in Scenario I. In case the component is included, it is shown by the mark ✓, and otherwise by the mark ✗.

from the proposed architecture affects the key metrics in Scenario I. The changes in SR illustrate how each element of our design contributes to the performance of our proposed method. The results show that all the reward components  $r_{do,t}$ ,  $r_{so,t}$  and  $r_{disp,t}$  have a significant impact on the performance of our method, while the impact of  $r_{disp,t}$  on the policy is more prominent. This highlights the importance of guiding the robot’s trajectory not only to avoid obstacles but also to make progress toward the target efficiently. We see that computing the similarity score across dynamic obstacles from their predicted trajectories has at least 7% higher SR and 1m lower PL. Tab. II shows that the policy model without utilizing partial observation of current flow shows

a 19% drop in SR and almost a 7m increase in PL. The reason is that when the robot is aware of current flow, it can steer in the directions where the path can be minimally affected by external forces and has a higher expected return in the long term.

## V. CONCLUSION

In this paper, we proposed a learning-based path planner for sensor-based USV navigation in marine environments with no prior knowledge about the environment. We further propose a transformer-based deep policy method and a training curriculum for marine navigation with dense and highly interactive obstacles and spatially variable current flow. Our work suggests that reasoning about an agent's interaction with current flow disturbances is an essential step toward smooth USV navigation. Compared to the Q-learning-based planner, the proposed method has a more stable performance and higher success rate. In particular, our method takes advantage of well-selected input features, an attention-based structure, and a carefully designed reward function. These allow the model to effectively balance collision avoidance with robustness to external disturbance while navigating towards the goal. Our work has the following limitations, which open up directions for future work. (1) The simulated trajectories of dynamic obstacles in the marine environment are far from realistic. To improve real-world performance, we need a better model or a dataset of real vessel navigation. (2) Our assumption that current flow never affects the dynamic obstacles does not hold. Thus, future work needs to incorporate the effect of the current disturbance of the dynamic obstacles. (3) Our results might be highly dependent on the accuracy of the current flow. Using methods that are more robust to the noise information can be addressed elsewhere. (4) Using time-varying current flow in place of the spatially variable current flow improves the adaptability and robustness of navigation policies for USVs in real-world settings. (5) Extension of the policies learned in simulation to real robot hardware can be a focus of future study.

## REFERENCES

- [1] A. Vagale, R. Ouchekh, R. T. Bye, O. L. Osen, and T. I. Fossen, "Path planning and collision avoidance for autonomous surface vehicles i: a review," *Journal of Marine Science and Technology*, pp. 1–15, 2021.
- [2] I. M. Organization, "Convention on the international regulations for preventing collisions at sea, 1972 (colregs)," 1972.
- [3] X. Lin, J. McConnell, and B. Englot, "Robust unmanned surface vehicle navigation with distributional reinforcement learning," in *2023 IEEE/RSJ International Conference on Intelligent Robots and Systems (IROS)*. IEEE, 2023, pp. 6185–6191.
- [4] C. Chen, Y. Liu, S. Kreiss, and A. Alahi, "Crowd-robot interaction: Crowd-aware robot navigation with attention-based deep reinforcement learning," in *2019 international conference on robotics and automation (ICRA)*. IEEE, 2019, pp. 6015–6022.
- [5] V. Ashish, "Attention is all you need," *Advances in neural information processing systems*, vol. 30, p. I, 2017.
- [6] J. Devlin, "Bert: Pre-training of deep bidirectional transformers for language understanding," *arXiv preprint arXiv:1810.04805*, 2018.
- [7] A. Dosovitskiy, L. Beyer, A. Kolesnikov, D. Weissenborn, X. Zhai, T. Unterthiner, M. Dehghani, M. Minderer, G. Heigold, S. Gelly, *et al.*, "An image is worth 16x16 words: Transformers for image recognition at scale," *arXiv preprint arXiv:2010.11929*, 2020.
- [8] L. Dong, S. Xu, and B. Xu, "Speech-transformer: a no-recurrence sequence-to-sequence model for speech recognition," in *2018 IEEE international conference on acoustics, speech and signal processing (ICASSP)*. IEEE, 2018, pp. 5884–5888.
- [9] S. Hochreiter and J. Schmidhuber, "Long short-term memory," *Neural computation*, vol. 9, no. 8, pp. 1735–1780, 1997.
- [10] M. Hausknecht and P. Stone, "Deep recurrent q-learning for partially observable mdps," in *2015 aaai fall symposium series*, 2015.
- [11] S. Liu, P. Chang, Z. Huang, N. Chakraborty, K. Hong, W. Liang, D. L. McPherson, J. Geng, and K. Driggs-Campbell, "Intention aware robot crowd navigation with attention-based interaction graph," in *2023 IEEE International Conference on Robotics and Automation (ICRA)*. IEEE, 2023, pp. 12 015–12 021.
- [12] S. Liu, P. Chang, W. Liang, N. Chakraborty, and K. Driggs-Campbell, "Decentralized structural-rnn for robot crowd navigation with deep reinforcement learning," in *2021 IEEE international conference on robotics and automation (ICRA)*. IEEE, 2021, pp. 3517–3524.
- [13] Y. F. Chen, M. Liu, M. Everett, and J. P. How, "Decentralized non-communicating multiagent collision avoidance with deep reinforcement learning," in *2017 IEEE international conference on robotics and automation (ICRA)*. IEEE, 2017, pp. 285–292.
- [14] M. Everett, Y. F. Chen, and J. P. How, "Motion planning among dynamic, decision-making agents with deep reinforcement learning," in *2018 IEEE/RSJ International Conference on Intelligent Robots and Systems (IROS)*. IEEE, 2018, pp. 3052–3059.
- [15] C. Chen, S. Hu, P. Nikdel, G. Mori, and M. Savva, "Relational graph learning for crowd navigation," in *2020 IEEE/RSJ International Conference on Intelligent Robots and Systems (IROS)*. IEEE, 2020, pp. 10 007–10 013.
- [16] K. D. Katyal, G. D. Hager, and C.-M. Huang, "Intent-aware pedestrian prediction for adaptive crowd navigation," in *2020 IEEE International Conference on Robotics and Automation (ICRA)*. IEEE, 2020, pp. 3277–3283.
- [17] X. Lin, Y. Huang, F. Chen, and B. Englot, "Decentralized multi-robot navigation for autonomous surface vehicles with distributional reinforcement learning," in *2024 IEEE International Conference on Robotics and Automation (ICRA)*. IEEE, 2024.
- [18] D. Fox, W. Burgard, and S. Thrun, "The dynamic window approach to collision avoidance," *IEEE Robotics & Automation Magazine*, vol. 4, no. 1, pp. 23–33, 1997.
- [19] M. Hoy, A. S. Matveev, and A. V. Savkin, "Algorithms for collision-free navigation of mobile robots in complex cluttered environments: a survey," *Robotica*, vol. 33, no. 3, pp. 463–497, 2015.
- [20] A. V. Savkin and C. Wang, "Seeking a path through the crowd: Robot navigation in unknown dynamic environments with moving obstacles based on an integrated environment representation," *Robotics and Autonomous Systems*, vol. 62, no. 10, pp. 1568–1580, 2014.
- [21] Z. Xie, P. Xin, and P. Dames, "Towards safe navigation through crowded dynamic environments," in *2021 IEEE/RSJ International Conference on Intelligent Robots and Systems (IROS)*. IEEE, 2021, pp. 4934–4940.
- [22] R. Song, Y. Liu, and R. Bucknall, "Smoothed a\* algorithm for practical unmanned surface vehicle path planning," *Applied Ocean Research*, vol. 83, pp. 9–20, 2019.
- [23] Y. Singh, S. Sharma, R. Sutton, D. Hatton, and A. Khan, "Feasibility study of a constrained dijkstra approach for optimal path planning of an unmanned surface vehicle in a dynamic maritime environment," in *2018 IEEE International Conference on Autonomous Robot Systems and Competitions (ICARSC)*. IEEE, 2018, pp. 117–122.
- [24] Y. Liu, R. Song, R. Bucknall, and X. Zhang, "Intelligent multi-task allocation and planning for multiple unmanned surface vehicles (usvs) using self-organising maps and fast marching method," *Information Sciences*, vol. 496, pp. 180–197, 2019.
- [25] S. M. LaValle and J. J. Kuffner Jr, "Randomized kinodynamic planning," *The international journal of robotics research*, vol. 20, no. 5, pp. 378–400, 2001.
- [26] O. Khatib, "Real-time obstacle avoidance for manipulators and mobile robots," *The international journal of robotics research*, vol. 5, no. 1, pp. 90–98, 1986.
- [27] J. Van den Berg, M. Lin, and D. Manocha, "Reciprocal velocity obstacles for real-time multi-agent navigation," in *2008 IEEE international conference on robotics and automation*. Ieee, 2008, pp. 1928–1935.
- [28] S. J. Guy, J. Chhugani, C. Kim, N. Satish, M. Lin, D. Manocha, and P. Dubey, "Clearpath: highly parallel collision avoidance for multi-agent simulation," in *Proceedings of the 2009 ACM SIG-*

- GRAPH/Eurographics Symposium on Computer Animation, 2009, pp. 177–187.
- [29] J. Van Den Berg, S. J. Guy, M. Lin, and D. Manocha, “Reciprocal n-body collision avoidance,” in *Robotics Research: The 14th International Symposium ISRR*. Springer, 2011, pp. 3–19.
- [30] J. Alonso-Mora, A. Breitenmoser, M. Ruffi, P. Beardsley, and R. Siegwart, “Optimal reciprocal collision avoidance for multiple non-holonomic robots,” in *Distributed autonomous robotic systems: The 10th international symposium*. Springer, 2013, pp. 203–216.
- [31] P. Fiorini and Z. Shiller, “Motion planning in dynamic environments using velocity obstacles,” *The international journal of robotics research*, vol. 17, no. 7, pp. 760–772, 1998.
- [32] P. Trautman and A. Krause, “Unfreezing the robot: Navigation in dense, interacting crowds,” in *2010 IEEE/RSJ International Conference on Intelligent Robots and Systems*. IEEE, 2010, pp. 797–803.
- [33] Y. Chen, C. Liu, B. E. Shi, and M. Liu, “Robot navigation in crowds by graph convolutional networks with attention learned from human gaze,” *IEEE Robotics and Automation Letters*, vol. 5, no. 2, pp. 2754–2761, 2020.
- [34] L. Liu, D. Dugas, G. Cesari, R. Siegwart, and R. Dubé, “Robot navigation in crowded environments using deep reinforcement learning,” in *2020 IEEE/RSJ International Conference on Intelligent Robots and Systems (IROS)*. IEEE, 2020, pp. 5671–5677.
- [35] V. Zambaldi, D. Raposo, A. Santoro, V. Bapst, Y. Li, I. Babuschkin, K. Tuyls, D. Reichert, T. Lillicrap, E. Lockhart, *et al.*, “Deep reinforcement learning with relational inductive biases,” in *International conference on learning representations*, 2019.
- [36] L. C. Melo, “Transformers are meta-reinforcement learners,” in *international conference on machine learning*. PMLR, 2022, pp. 15 340–15 359.
- [37] E. Parisotto, F. Song, J. Rae, R. Pascanu, C. Gulcehre, S. Jayakumar, M. Jaderberg, R. L. Kaufman, A. Clark, S. Noury, *et al.*, “Stabilizing transformers for reinforcement learning,” in *International conference on machine learning*. PMLR, 2020, pp. 7487–7498.
- [38] R. Loynd, R. Fernandez, A. Celikyilmaz, A. Swaminathan, and M. Hausknecht, “Working memory graphs,” in *International conference on machine learning*. PMLR, 2020, pp. 6404–6414.
- [39] K. Irie, I. Schlag, R. Csordás, and J. Schmidhuber, “Going beyond linear transformers with recurrent fast weight programmers,” *Advances in neural information processing systems*, vol. 34, pp. 7703–7717, 2021.
- [40] K. Esslinger, R. Platt, and C. Amato, “Deep transformer q-networks for partially observable reinforcement learning,” *arXiv preprint arXiv:2206.01078*, 2022.
- [41] L. Chen, K. Lu, A. Rajeswaran, K. Lee, A. Grover, M. Laskin, P. Abbeel, A. Srinivas, and I. Mordatch, “Decision transformer: Reinforcement learning via sequence modeling,” *Advances in neural information processing systems*, vol. 34, pp. 15 084–15 097, 2021.
- [42] X. Xiao, T. Zhang, K. M. Choromanski, T.-W. E. Lee, A. Francis, J. Varley, S. Tu, S. Singh, P. Xu, F. Xia, *et al.*, “Learning model predictive controllers with real-time attention for real-world navigation,” in *Conference on Robot Learning*. PMLR, 2023, pp. 1708–1721.
- [43] A. Banino, A. P. Badia, J. Walker, T. Scholtes, J. Mitrovic, and C. Blundell, “Coberl: Contrastive bert for reinforcement learning,” *arXiv preprint arXiv:2107.05431*, 2021.
- [44] L. Fan, G. Wang, Y. Jiang, A. Mandlekar, Y. Yang, H. Zhu, A. Tang, D.-A. Huang, Y. Zhu, and A. Anandkumar, “Minedojo: Building open-ended embodied agents with internet-scale knowledge,” *Advances in Neural Information Processing Systems*, vol. 35, pp. 18 343–18 362, 2022.
- [45] S. Li, X. Puig, C. Paxton, Y. Du, C. Wang, L. Fan, T. Chen, D.-A. Huang, E. Akyürek, A. Anandkumar, *et al.*, “Pre-trained language models for interactive decision-making,” *Advances in Neural Information Processing Systems*, vol. 35, pp. 31 199–31 212, 2022.
- [46] Y. Ma, M. Hu, and X. Yan, “Multi-objective path planning for unmanned surface vehicle with currents effects,” *ISA transactions*, vol. 75, pp. 137–156, 2018.
- [47] J. Meng, Y. Liu, R. Bucknall, W. Guo, and Z. Ji, “Anisotropic gmp2: A fast continuous-time gaussian processes based motion planner for unmanned surface vehicles in environments with ocean currents,” *IEEE Transactions on Automation Science and Engineering*, vol. 19, no. 4, pp. 3914–3931, 2022.
- [48] W. Lan, X. Jin, T. Wang, and H. Zhou, “Improved rrt algorithms to solve path planning of multi-glider in time-varying ocean currents,” *IEEE Access*, vol. 9, pp. 158 098–158 115, 2021.
- [49] W. Sun, P. Tsiotras, T. Lolla, D. N. Subramani, and P. F. Lermusiaux, “Multiple-pursuer/one-evader pursuit–evasion game in dynamic flow-fields,” *Journal of guidance, control, and dynamics*, vol. 40, no. 7, pp. 1627–1637, 2017.
- [50] M. Xi, J. Yang, J. Wen, H. Liu, Y. Li, and H. H. Song, “Comprehensive ocean information-enabled auv path planning via reinforcement learning,” *IEEE Internet of Things Journal*, vol. 9, no. 18, pp. 17 440–17 451, 2022.
- [51] M. Khalid, L. Pénard, and E. Mémin, “Optical flow for image-based river velocity estimation,” *Flow Measurement and Instrumentation*, vol. 65, pp. 110–121, 2019.
- [52] ArduPilot Dev Team, “Object avoidance with bendy ruler for copter,” <https://ardupilot.org/copter/docs/common-aa-bendyruler.html>, 2024, accessed: 2024-09-21.
- [53] D. J. Acheson, *Elementary fluid dynamics*. Oxford University Press, 1990.
- [54] T. Lolla, P. F. Lermusiaux, M. P. Ueckermann, and P. J. Haley, “Time-optimal path planning in dynamic flows using level set equations: theory and schemes,” *Ocean Dynamics*, vol. 64, pp. 1373–1397, 2014.
- [55] P. Long, T. Fan, X. Liao, W. Liu, H. Zhang, and J. Pan, “Towards optimally decentralized multi-robot collision avoidance via deep reinforcement learning,” in *2018 IEEE international conference on robotics and automation (ICRA)*. IEEE, 2018, pp. 6252–6259.
- [56] X. Fan, Y. Guo, H. Liu, B. Wei, and W. Lyu, “Improved artificial potential field method applied for auv path planning,” *Mathematical Problems in Engineering*, vol. 2020, no. 1, p. 6523158, 2020.
- [57] W. Dabney, G. Ostrovski, D. Silver, and R. Munos, “Implicit quantile networks for distributional reinforcement learning,” in *International conference on machine learning*. PMLR, 2018, pp. 1096–1105.
- [58] M. G. Bellemare, W. Dabney, and R. Munos, “A distributional perspective on reinforcement learning,” in *International conference on machine learning*. PMLR, 2017, pp. 449–458.
- [59] V. Mnih, K. Kavukcuoglu, D. Silver, A. A. Rusu, J. Veness, M. G. Bellemare, A. Graves, M. Riedmiller, A. K. Fidjeland, G. Ostrovski, *et al.*, “Human-level control through deep reinforcement learning,” *nature*, vol. 518, no. 7540, pp. 529–533, 2015.
- [60] J. Schulman, F. Wolski, P. Dhariwal, A. Radford, and O. Klimov, “Proximal policy optimization algorithms,” *arXiv preprint arXiv:1707.06347*, 2017.